Available online at www.sciencedirect.com

ScienceDirect

IFAC Papers Online CONFERENCE PAPER ARCHIVE

IFAC PapersOnLine 56-2 (2023) 3930–3935

Bifurcating vector fields driven by time-scale separated motivational dynamics

Kleio Baxevani and Herbert G. Tanner

Center for Autonomous and Robotic Systems

University of Delaware, USA; email: {kleiobax, btanner}@udel.edu.

Abstract: Dynamical systems can be designed to exhibit a range of distinct behaviors, which all arise from the same set of continuous dynamics when the latter bifurcates, triggered by a switch in one of its scalar parameters. Building on recent advances that introduce motivation and value dynamics as an efficient way to design multi-behavioral systems, this paper lifts some of the existing restrictions on what kind of planar vector fields can be combined to produce bifurcations. This relaxation enriches the class of dynamical systems that such an approach applies, and gives rise to new behaviors. The paper identifies new analytical conditions under which this new set of planar vector fields can undergo Hopf bifurcations and result in a multi-behavioral system. Numerical simulations and experimental results confirm the theoretical predictions for the existence of the Hopf bifurcations and the applicability of the theory in real systems.

Keywords: Control of bifurcation and chaos, Adaptive control, Switching stability and control, Artificial vector fields

1. INTRODUCTION

The overarching goal that motivates this work, is to establish engaging play-based social interaction between a collection of inexpensive, commercial-off-the-shelfs (COTSs) toy robots (Fig. 1) and children, in order to serve specific pediatric rehabilitation objectives (Kokkoni et al., 2020). Indeed, as observed by Kokkoni et al. (2017) one robot control objective that may lead to engaging robot-child interaction is enabling the robot to adapt to the child's response. Thus, the system that is able to exhibit multiple behaviors and switch between them depending on its playmate's reactions, could contribute to attracting and preserving attention, focus, and active engagement.

Low-cost robots have a higher probability of adoption and penetration into homes where children with special needs spend most of their time. Such low-cost mobile robotic toys are likely to have limited computation, communication, and sensing capabilities. Accordingly, their control features would also be limited to basic motion primitives and their communication functions be confined to bluetooth. Yet such inexpensive devices are expected to be able to recover fast and unharmed from collisions, drops, and throws, and are thus inherently robust for gameplay. In principle, and among several options, a low-level controller for such a robot during child-robot interaction can be realized as artificial vector fields (Tanner and Boddu, 2012) which steers the robot to follow a specific behavior. The robot would have to follow the field's flow lines, and can not only implement obstacle avoidance constraints, but also conform to complex desired objectives associated with human-robot interaction (Zehfroosh and Tanner, 2022). In this context, a robotic toy becomes interesting and engaging if it can respond to the child's behavior with a *range* of its own appropriate behaviors.

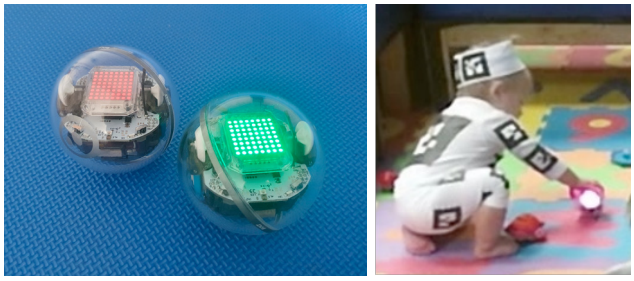

(a) Sphero Bolt™ (b) Infant with Sphero

Fig. 1. (a) A commercially available educational robotic toy. (b) Snapshot of infant physically interacting with Sphero in play-based activities (Kouvoutsakis et al., 2022).

1.1 Related work

Dynamical systems that can selectively exhibit multiple dynamical behaviors emerge in numerous applications in robotics, from legged locomotion (Veer et al., 2019) to motion planning (Kress-Gazit et al., 2007; Fainekos et al., 2005), and even pediatric rehabilitation (Zehfroosh and Tanner, 2019).

One traditional path to model multi-behavioral systems is through a switching (Liberzon, 2003) or hybrid control approach (Goebel et al., 2012; Lygeros et al., 2003; van der Schaft and Schumacher, 2000), in which each behavior/mode can be represented through distinct closed-loop continuous dynamics. Transitions between different modes can be triggered either by a piecewise constant switching signal (Liberzon, 2003), which can be random or deliberate (based on specific timed or state-based events), or some discrete (Goebel et al., 2012; Lygeros et al., 2003), possibly temporal (van der Schaft and Schumacher, 2000) logic. However, the stability analysis of such systems is not trivial (Valbuena and Tanner, 2012), especially in the case of multiple equilibria that may not be isolated (Veer et al., 2019). One well-known stability analysis approach for

⋆ This work is supported by NSF's SCH program via award #2014264.

10.1016/j.ifacol.2023.10.1842

hybrid systems involves, for example, multiple Lyapunov functions (Branicky, 1998), intuitively one for each mode dynamics; however, establishing the required conditions across mode switching is not straightforward in general.

Arguably, analysis can be simpler if modes share the *same* continuous dynamics structure, demarcated by some constant system parameters. One may wonder how the same set of differential equations can exhibit distinctly different dynamical behaviors, and yet this is the case in many instances encountered in bifurcation theory (Reverdy and Koditschek, 2018). In this paradigm, a finite set of continuous (navigation) vector fields are continuously blended through a time-varying weighted superposition, in which the weights follow some (motivational) dynamics of their own. Similar methods have been also utilized to multi-agent systems for adapting the behavior of one agent based on its neighbors' behaviors (Zhong and Leonard, 2019).

The approach reported in this paper follows the aforementioned motivational dynamics paradigm for behavior switching. By extending earlier work in this direction that models the system in a pitchfork bifurcation setting (Baxevani and Tanner, 2021, 2023; Reverdy, 2019), this paper frames the bifurcation problem in a singular perturbation framework. In this model, an extra set of dynamics, the so called *value dynamics*, is added to the system (Reverdy and Koditschek, 2018). The value dynamics is a positive metric associated with each task/vector field and the conceptual meaning of this set is the urgency to follow each of the component vector field.

1.2 Contribution and Paper Organization

The more general (relatively to the ones that have been reported in literature) case where the component vector field attractors are not isolated, is far more complex and challenging as it has been stated (Thompson and Reverdy, 2019). This paper addresses directly this case. Its contribution is a general approach to analyzing the emergence of bifurcations in such complex scenarios, and a demonstration of how the theory can be used to enable a robot exhibit multiple dynamic behaviors and rapidly switch among them, while maintaining the same underlying set of differential equations.

The rest of the paper is organized as follows. Section 2 introduces mathematical preliminaries and definitions. Section 3 formalizes the mathematical problem considered, and leads to Section 4 that presents the main results of the paper. Numerical and experimental results confirming the theoretical predictions are presented in Section 5. The paper concludes by highlighting a few remarks of this work and some future directions in Section 6.

2. PROBLEM FORMULATION

Consider an agent moving on the plane, located at (x_r, y_r, θ_r) and having unicycle dynamics of the form

$$\dot{x}_r = v\,\cos\theta_r \qquad \dot{y}_r = v\,\sin\theta_r \qquad \dot{\theta}_r = \omega \ , \tag{1}$$

where v and ω are the linear and angular speed inputs, respectively, and assume that it has an output defined as

$$\begin{bmatrix}\eta_x\\ \eta_y\end{bmatrix} \triangleq h\big(x_r, y_r\big) \triangleq \begin{bmatrix}x_r + \varepsilon\cos\theta_r\\ y_r + \varepsilon\sin\theta_r\end{bmatrix} \tag{2}$$

for some small $\varepsilon > 0$. It is well known that this system is output feedback linearizable (Valbuena and Tanner, 2015); the feedback linearization process will not be repeated here for reasons of brevity, and we will assume that the output dynamics is in the form of a single integrator

$$\dot{\eta}_x = \nu_x \qquad\qquad \dot{\eta}_y = \nu_y \ , \tag{3}$$

with ν_x and ν_y the new, transformed control inputs which can be expressed as

$$\begin{bmatrix}\eta_x\\ \eta_y\end{bmatrix} = \begin{bmatrix}\cos\theta_r & -\varepsilon\sin\theta_r\\ \sin\theta_r & \varepsilon\cos\theta_r\end{bmatrix}\begin{bmatrix}v\\ \omega\end{bmatrix} \ .$$

The control objective is to design a feedback law so that with the choice of a *single scalar parameter* and without otherwise changing its dynamics, (1) can converge to either one of three different limit cycles or a stable node attractor.

3. TECHNICAL PRELIMINARIES

3.1 General Formulation

Let $w = (x, y) \in \mathcal{D} \subseteq \mathbb{R}^2$, and consider *planar vector fields* $F_i(w) : \mathcal{D} \to T\mathcal{D}$, for $i \in I \subset \mathbb{N}$. Each vector field has an *associated (Lyapunov) function* $f_i : \mathcal{D} \to \mathbb{R}$ for which it is known that

$$\dot{f}_i = \nabla^\intercal f_i \, F_i \leq 0 \ .$$

(Equality on the right holds when the expression is evaluated at stationary points of F_i.)

Let m_1 and m_2 be scalar variables in $[0, 1]$ representing the degree to which the dynamical behavior captured by F_i manifests itself in the system. These two variables define the *motivation state* of the system; they can have dynamics of their own and thus evolve over time.

The scalar variables v_i, referred to as *values*, encode the importance of each dynamical behavior F_i. The value of a component vector field F_i increases as the urgency of the task/behavior encoded in F_i increases. As with the motivation state, the value state has its own dynamics that will be introduced shortly.

Based on F_i and m_i, the *navigation dynamics* is defined as a dynamical system formed by the convex combination of F_i, using the motivation state variables m_i as weights:

$$\dot{w} = m_1(t) \cdot F_1(w) + m_2(t) \cdot F_2(w) \ . \tag{4}$$

The *value dynamics* is defined as

$$\dot{v}_i = \tfrac{1}{\lambda_i}(f_i - v_i) \ , \tag{5}$$

where λ_i is a scale parameter. Define now the *undecided motivation state*

$$m_U \triangleq 1 - \sum_i m_i \ ,$$

and let $\sigma \in \mathbb{R}_+$ be the *bifurcation parameter*, and v_i^* is a positive real gain. Then the *motivation dynamics* of the system inspired by the decision-making behavior in honeybee swarms (Pais et al. (2013)) can be defined as

$$\dot{m}_i = v_i^* v_i m_U - m_i\big[\tfrac{1}{v_i^* v_i} - v_i^* v_i m_U + \sigma(1 - m_i - m_U)\big] \ . \tag{6}$$

With this dynamical system setup in place, define the set of *mean-difference* coordinates

$$\bar{F} = \tfrac{F_1(w)+F_2(w)}{2} \qquad \Delta F = F_1(w) - F_2(w) \tag{7a}$$

$$\bar{f} = \tfrac{f_1(w)+f_2(w)}{2} \qquad \Delta f = f_1(w) - f_2(w) \tag{7b}$$

$$\bar{m} = \tfrac{m_1(t)+m_2(t)}{2} \qquad \Delta m = m_1(t) - m_2(t) \tag{7c}$$

$$\bar{v} = \tfrac{v_1(t)+v_2(t)}{2} \qquad \Delta v = v_1(t) - v_2(t) \ , \tag{7d}$$

which can be combined into a stack vector

$$q = (x, y, \bar{m}, \Delta m, \bar{v}, \Delta v)^\intercal \ . \tag{8}$$

3.2 Particularization

Now assume, for clarity of presentation, that we have just two planar vector fields of the form:

$$\dot{x} = r(y - y_{ci}) - (x - x_{ci})\big[(x - x_{ci})^2 + (y - y_{ci})^2 - r^2\big]$$
$$\dot{y} = -r(x - x_{ci}) - (y - y_{ci})\big[(x - x_{ci})^2 + (y - y_{ci})^2 - r^2\big] \ ,$$

which each produces a circular attractive limit cycle centered at (x_{ci}, y_{ci}) and with radius $r > 0$.

Without loss of generality, we can simplify the analysis assuming: $(x_{c_1}, y_{c_1}) = (0, 0)$, $y_{c_2} = 0$, and $x_{c_2} \triangleq x_{\rm dis} > 0$, which reduces the expressions of the vector fields to the form:

$$F_1 : \begin{cases} \dot{x} = ry - x(x^2 + y^2 - r^2) \\ \dot{y} = -rx - y(x^2 + y^2 - r^2) \end{cases} \tag{9a}$$

$$F_2 : \begin{cases} \dot{x} = ry - (x - x_{\rm dis})[(x - x_{\rm dis})^2 + y^2 - r^2] \\ \dot{y} = -r(x - x_{\rm dis}) - y[(x - x_{\rm dis})^2 + y^2 - r^2] \ . \end{cases} \tag{9b}$$

For each one of the vector fields above we can define an *associated Lyapunov function* $f_i(x, y)$ as follows:

$$f_1(x, y) = \tfrac{1}{4}(x^2 + y^2 - r^2)^4 \tag{10a}$$
$$f_2(x, y) = \tfrac{1}{4}\big[(x - x_{\rm dis})^2 + y^2 - r^2\big]^4 \ . \tag{10b}$$

The dynamics of the mean-difference coordinates induced by (4)–(6) after substituting (9) and (10) can now be expressed as—with a slight abuse of notation where we use $(\dot{x}, \dot{y})$ to express the two components of the blended vector field $\dot{w}$ in (4):

$$\begin{aligned} \dot{w}_1 \equiv \dot{x} = {} & \Delta m\, x_{\rm dis}(0.5r^2 - 1.5x^2 + 1.5x_{\rm dis}x - 0.5y^2 \\ & - 0.5x_{\rm dis}^2) + \bar{m}(r^2(2x - x_{\rm dis}) + 2ry - 2x^3 \\ & + 3x^2x_{\rm dis} - 2xy^2 - 3x_{\rm dis}^2x + y^2x_{\rm dis} + x_{\rm dis}^3) \end{aligned} \tag{11a}$$

$$\begin{aligned} \dot{w}_2 \equiv \dot{y} = {} & \Delta m\, x_{\rm dis}(-0.5r - xy + 0.5yx_{\rm dis}) \\ & + \bar{m}(2r^2y - 2rx + rx_{\rm dis} - 2x^2y \\ & + 2xyx_{\rm dis} - 2y^3 - yx_{\rm dis}^2) \end{aligned} \tag{11b}$$

$$\begin{aligned} \dot{\bar{m}} = {} & 0.25\sigma(\Delta m^2 - 4\bar{m}^2) + \frac{0.25\Delta m\Delta v(1 - 2\bar{m})}{\epsilon_m} \\ & - \frac{0.5\epsilon_m(\Delta m + 2\bar{m})}{2\bar{v} + \Delta v} + \frac{0.5\epsilon_m(\Delta m - 2\bar{m})}{2\bar{v} - \Delta v} \\ & + \frac{\bar{v}(1 - 2\bar{m})(\bar{m} + 1)}{\epsilon_m} \end{aligned} \tag{11c}$$

$$\begin{aligned} \tfrac{{\rm d}\Delta m}{{\rm d}t} = {} & -\frac{\epsilon_m(\Delta m + 2\bar{m})}{2\bar{v} + \Delta v} - \frac{\epsilon_m(\Delta m - 2\bar{m})}{2\bar{v} - \Delta v} \\ & - \frac{\bar{v}\Delta m(2\bar{m} - 1)}{\epsilon_m} - \frac{\Delta v(2\bar{m}^2 + \bar{m} - 1)}{\epsilon_m} \end{aligned} \tag{11d}$$

$$\dot{\bar{v}} = \tfrac{1}{\epsilon_v}(\bar{f} - \bar{v}) \tag{11e}$$

$$\tfrac{{\rm d}\Delta v}{{\rm d}t} = \tfrac{1}{\epsilon_v}(\Delta f - \Delta v) \ , \tag{11f}$$

setting $v_1^* = v_2^* = v^*, \lambda_1 = \lambda_2 = \lambda$.

4. MAIN RESULTS

In this section we demonstrate how one can ensure the existence of threshold values for parameter σ that will ensure the existence of a Hopf bifurcation in (11). The idea now is to align the (x, y) velocity of (1) to the dynamics of (w_1, w_2), and by doing so, steer the robot along the flow lines of the resulting time-varying vector field. Whenever the underlying vector field undergoes a bifurcation, the closed-loop dynamic behavior of robot would switch. To this end, define $\epsilon_m = 1/v^*$ and $\epsilon_v = 1/\lambda$, and recognize (11) as a *singular perturbation* system with $\epsilon_m, \epsilon_v \in \mathbb{R}_+$ being (independent) infinitesimally small parameters. To analyze (11) consider first the time-scale decomposition between the subsystem of the pair of "ultra-fast" variables $(z_1, z_2) \triangleq (\bar{v}, \Delta v)$ in (11e)–(11f), and that of the fast variable $\bar{m}$ of (11c). In the limit as $\epsilon_v \to 0$, notice that ultra-fast $(z_1, z_2) \to (\bar{f}, \Delta f)$ exponentially, and the dynamics of the fast (but slower than z_i) $\bar{m}$ reduces to

$$\begin{aligned} \dot{\bar{m}} = {} & 0.25\sigma(\Delta m^2 - 4\bar{m}^2) + \frac{0.25\Delta m\Delta f(1 - 2\bar{m})}{\epsilon_m} \\ & - \frac{0.5\epsilon_m(\Delta m + 2\bar{m})}{2\bar{f} + \Delta f} + \frac{0.5\epsilon_m(\Delta m - 2\bar{m})}{2\bar{f} - \Delta f} \\ & + \frac{\bar{f}(1 - 2\bar{m})(\bar{m} + 1)}{\epsilon_m} \ . \end{aligned} \tag{12}$$

We will now replace the fast variable $\bar{m}$ with

$$\tilde{z}_1 \triangleq \frac{1 - 2\bar{m}}{\epsilon_m}$$

to obtain this fast dynamics in the form:

$$\begin{aligned} \epsilon_m\dot{\tilde{z}}_1 = {} & -0.5\sigma(\Delta m^2 - (1 - \epsilon_m\tilde{z}_1)^2) - 0.5\Delta m\Delta f\tilde{z}_1 \\ & + \frac{\epsilon_m(\Delta m + 1 - \epsilon_m\tilde{z}_1)}{2\bar{f} + \Delta f} - \frac{\epsilon_m(\Delta m - 1 + \epsilon_m\tilde{z}_1)}{2\bar{f} - \Delta f} \\ & - 2\bar{f}\tilde{z}_1(\tfrac{1 - \epsilon_m\tilde{z}_1}{2} + 1) \ , \end{aligned} \tag{13}$$

which in the limit $\epsilon_m \to 0$ yield a quasi-static steady state where

$$\tilde{z}_1 \to -\frac{\sigma(\Delta m^2 - 1)}{\Delta m\Delta f + 6\bar{f}} \ . \tag{14}$$

Now rename $\Delta m := w_3$ and group the slow dynamics of x, y, and Δm of (11a), (11b), and (11d), respectively, in the form:

$$\begin{aligned} \dot{w}_1 = {} & w_3x_{\rm dis}\big(\tfrac{1}{2}r^2 - \tfrac{3}{2}w_1^2 + \tfrac{3}{2}w_1x_{\rm dis} - \tfrac{1}{2}w_2^2 - \tfrac{1}{2}x_{\rm dis}^2\big) \\ & + \tfrac{1}{2}\big[r^2(2w_1 - x_{\rm dis}) + 2rw_2 - 2w_1^3 + 3w_1^2x_{\rm dis} \\ & - 2w_1w_2^2 - 3w_1x_{\rm dis}^2 + w_2^2w_1 + x_{\rm dis}^3\big] \end{aligned} \tag{15a}$$

$$\begin{aligned} \dot{w}_2 = {} & -w_3x_{\rm dis}(\tfrac{1}{2}r + w_1w_2 - \tfrac{1}{2}w_2x_{\rm dis}) \\ & + \tfrac{1}{2}\big(2r^2w_2 - 2rw_1 + rx_{\rm dis} - 2w_1^2\tilde{w}_2 \\ & + 2w_1w_2x_{\rm dis} - 2w_2^3 - w_2x_{\rm dis}^2\big) \end{aligned} \tag{15b}$$

$$\dot{w}_3 = -\bar{f}w_3\tfrac{\sigma(w_3^2 - 1)}{w_3\Delta f + 3\bar{f}} - \tfrac{3}{4}\Delta f\frac{\sigma(w_3^2 - 1)}{w_3\Delta f + 3\bar{f}} \ . \tag{15c}$$

Definition 1. *An equilibrium w_d of* (15) *is called a deadlock if* $w_3 = 0$. ◇

Proposition 1. *Given* (9)–(10)*, there is a deadlock for* (15) *at* $w_d = (x_{\rm dis}/2, 0, 0)^\intercal$.

Proof. By direct derivation: at the deadlock, $w_{3_d} = 0$ (Definition 1). Given that $w_{3_d} = 0$ and should remain constant at w_d,

$$\begin{aligned} \tfrac{{\rm d}w_3}{{\rm d}t}\Big|_{w_3=0} = 0 \overset{(15)}{\implies} \Delta f = 0 \overset{(7b)(10)}{\implies} & (w_1^2 + w_2^2 - r^2)^2 \\ & = [(w_1 - x_{\rm dis})^2 + w_2^2 - r^2]^2 \ . \end{aligned} \tag{16}$$

One of the solutions of (16) is $\tilde{w}_{1_d} = x_{\rm dis}/2$. Substituting into (15) given that $\tilde{w}_d$ is an equilibrium yields

$$\frac{{\rm d}w_1}{{\rm d}t}\Big|_{w_d} = 0 \overset{(15)}{\implies} w_{2_d} = 0 \ ,$$

which suggests that $w_{2_d} = 0$ too. Therefore, the equilibrium coordinates are indeed $w_d = (x_{\text{dis}}/2, 0, 0)$. □

The Jacobian of the system vector field is a 3-dimensional matrix represented in the form

$$J(w) = \begin{bmatrix} J_{11} & J_{12} & J_{13} \\ J_{21} & J_{22} & J_{23} \\ J_{31} & J_{32} & J_{33} \end{bmatrix} \ , \tag{17}$$

which is naturally parameterized by x_{dis}, r, and σ, given (9) and (15). Let

$$J_d \triangleq J(w)\,|_{w=w_d} \ .$$

Proposition 2. *Under the following two conditions on the elements of the system's Jacobian* (17) *evaluated at the deadlock w_d, i.e., an equality constraint:*

$$\begin{aligned} &- J_{11}^2(J_{22}+J_{33}) - J_{22}^2(J_{11}+J_{33}) - J_{33}^2(J_{22}+J_{33}) \\ &+ J_{11}J_{12}J_{21} + J_{11}J_{13}J_{31} + J_{22}J_{23}J_{32} + J_{22}J_{12}J_{21} \\ &+ J_{33}J_{23}J_{32} + J_{33}J_{13}J_{31} + J_{12}J_{23}J_{31} + J_{21}J_{13}J_{32} \\ &- 2J_{11}J_{22}J_{33} = 0 \ , \end{aligned} \tag{18a}$$

and an inequality constraint:

$$tr\, J_d = J_{11} + J_{22} + J_{33} < 0 \ , \tag{18b}$$

J_d has two purely imaginary eigenvalues and one real negative eigenvalue.

Proof. The characteristic polynomial of (17) is

$$\lambda^3 - \text{tr}\, J_d \cdot \lambda^2 - \frac{(\text{tr} J_d)^2 - \text{tr}\, J_d^2}{2}\lambda - \det\, J_d \ . \tag{19}$$

A third-degree polynomial in λ with two purely imaginary roots $\lambda_{1,2} = \pm\alpha j \in \mathbb{I}$ and one real eigenvalue $\lambda_3 = \beta \in \mathbb{R}$ must have the general form

$$\lambda^3 - \beta\lambda^2 + \alpha^2\lambda - \alpha^2\beta \ . \tag{20}$$

Matching the coefficients of (19) and (20) one has:

$$\beta = \text{tr}\, J_d \tag{21a}$$

$$\alpha^2 = -\frac{(\text{tr} J_d)^2 - \text{tr}\, J_d^2}{2} \tag{21b}$$

$$\alpha^2\beta = \det\, J_d \ . \tag{21c}$$

Plugging (21a) and (21b) into (21c) yields

$$\frac{[(\text{tr} J_d)^2 - \text{tr}\, J_d^2]\,\text{tr}\, J_d}{2} + \det\, J_d = 0 \ ,$$

expansion of which gives (18a).

Condition (18b) comes directly from the assumed expression for the 3rd root, $\lambda_3 = \beta$, which in order to be negative, and in view of (21a),

$$\beta = \text{tr}\, J_d < 0 \ . \tag{22}$$

□

The left hand side of (18b) reduces to

$$\text{tr} J_d = -\frac{3}{16}\sigma + 2r^2 - x_{\text{dis}}^2 \ . \tag{23}$$

Condition (18a) is a 2nd order polynomial in σ and allows for two possible solutions which can be written with respect to x_{dis}, r in terms of a ratio between two polynomials N_1 and N_2:

$$\sigma_{1,2} = \frac{N_1(r, x_{\text{dis}})}{2N_2(r, x_{\text{dis}})} \ , \tag{24}$$

where N_2 is defined as

$$\begin{aligned} N_2(r, x_{\text{dis}}) \triangleq\ & a_5 r^{18} + a_6 r^{16} x_{\text{dis}}^2 + a_7 r^{14} x_{\text{dis}}^4 + a_8 r^{12} x_{\text{dis}}^6 \\ & + a_9 r^{10} x_{\text{dis}}^8 + a_{10} r^8 x_{\text{dis}}^{10} + a_{11} r^6 x_{\text{dis}}^{12} + a_{12} r^4 x_{\text{dis}}^{14} + a_{13} r^2 x_{\text{dis}}^{16} \end{aligned}$$

and N_1 is expressed in terms of two other expressions $P(r, x_{\text{dis}})$ and $Q(r, x_{\text{dis}})$, also involving polynomials, as

$$\begin{aligned} N_1(r, x_{\text{dis}}) \triangleq\ & \left[P(r, x_{\text{dis}}) \pm Q(r, x_{\text{dis}})\right] \\ & (a_1 r^8 - a_1 r^6 x_{\text{dis}}^2 + a_2 r^4 x_{\text{dis}}^4 + a_3 r^2 x_{\text{dis}}^6 + a_4 x_{\text{dis}}^8)^2 \ . \end{aligned}$$

The auxiliary expressions $P(r, x_{\text{dis}})$ and $Q(r, x_{\text{dis}})$ are themselves defined as

$$P(r, x_{\text{dis}}) \triangleq \frac{H_1(r, x_{\text{dis}})}{H_2(r, x_{\text{dis}})} \ ,$$

where

$$\begin{aligned} H_1(r, x_{\text{dis}}) \triangleq\ & p_1 r^{12} + p_2 r^{10} x_{\text{dis}}^2 + r^8\left(-p_1 x_{\text{dis}}^4 - x_{\text{dis}}^2\right) \\ & + r^6\left(p_1 x_{\text{dis}}^6 + p_3 x_{\text{dis}}^4\right) + r^4\left(p_4 x_{\text{dis}}^8 + p_5 x_{\text{dis}}^6\right) \\ & + r^2 x_{\text{dis}}^8\left(p_6 x_{\text{dis}}^2 + p_7\right) + p_8 x_{\text{dis}}^{12} \ , \end{aligned}$$

and

$$H_2(r, x_{\text{dis}}) \triangleq r^8 - r^6 x_{\text{dis}}^2 + p_9 r^4 x_{\text{dis}}^4 + p_{10} r^2 x_{\text{dis}}^6 + p_{11} x_{\text{dis}}^8 \ ,$$

while

$$Q(r, x_{\text{dis}}) \triangleq \sqrt{\tfrac{H_3(r, x_{\text{dis}})}{H_4(r, x_{\text{dis}})}} \ ,$$

where

$$H_4(r, x_{\text{dis}}) \triangleq (r^8 - r^6 x_{\text{dis}}^2 + p_9 r^4 x_{\text{dis}}^4 + p_{10} r^2 x_{\text{dis}}^6 + p_{11} x_{\text{dis}}^8)^2 \ ,$$

$$\begin{aligned} H_3(r, x_{\text{dis}}) \triangleq\ & q_1 r^{22} + r^{20}(x_{\text{dis}}^4 + q_3 x_{\text{dis}}^2) \\ & + r^{18}(q_4 x_{\text{dis}}^4 + q_5 x_{\text{dis}}^6) + r^{16}(q_6 x_{\text{dis}}^8 + q_7 x_{\text{dis}}^6 + x_{\text{dis}}^4) \\ & + r^{14}(q_8 x_{\text{dis}}^4 + q_9 x_{\text{dis}}^2 + q_{10}) x_{\text{dis}}^6 \\ & + r^{12}(q_{11} x_{\text{dis}}^4 + q_{12} x_{\text{dis}}^2 + q_{13}) x_{\text{dis}}^8 \\ & + r^{10}(q_{14} x_{\text{dis}}^4 + q_{15} x_{\text{dis}}^2 + q_{16}) x_{\text{dis}}^{10} \\ & + r^8(q_{17} x_{\text{dis}}^4 + q_{18} x_{\text{dis}}^2 + q_{19}) x_{\text{dis}}^{12} \\ & + r^6(q_{20} x_{\text{dis}}^4 + q_{21} x_{\text{dis}}^2 + q_{22}) x_{\text{dis}}^{14} \\ & + r^4(q_{23} x_{\text{dis}}^4 + q_{24} x_{\text{dis}}^2 + q_{25}) x_{\text{dis}}^{16} + r^2(q_{26} x_{\text{dis}}^2 + q_{27}) x_{\text{dis}}^{20} \ . \end{aligned}$$

The values for the coefficients in those expressions are given in Table 1.

i	a_i	p_i	q_i	q_{14+i}
1	0.75	$0.\bar{6}$	$-0.\bar{4}$	-0.50434
2	0.28125	$-0.\bar{3}$	$0.69\bar{4}$	-0.3125
3	-0.046875	0.75	$-1.\bar{3}$	0.187039
4	0.00292969	-0.236979	$3.\bar{2}$	0.134657
5	0.03125	-0.1875	-2.5	0.0585938
6	0.015625	0.0377604	3.88194	-0.0322401
7	-0.101563	0.015625	$-1.69\bar{4}$	-0.0207587
8	0.109375	-0.00227865	-3.44097	-0.00585938
9	-0.0598145	0.375	-0.559028	0.00359133
10	0.0196533	-0.0625	-1.5	0.00174967
11	-0.00405884	0.00390625	1.93989	0.000244141
12	0.000518799		1.00868	-0.000233968
13	-0.0000376701		0.9375	-0.0000627306
14			-0.730686	

Table 1. The values of the coefficients in polynomials N_1, N_2, H_1, H_2, H_3, and H_4.

When $Q(r, x_{\text{dis}}) < 0$, then the solutions (24) are complex and are therefore discarded —in this case no Hopf bifurcation can be triggered for the particular choice of (x_{dis}, r). For a Hopf bifurcation to exist, even when both solutions (24) are real, the

values of the system and bifurcation parameters should satisfy according to (18b)

$$\sigma < \frac{S_1(r, x_{\text{dis}})}{S_2(r, x_{\text{dis}})} \quad , \tag{25}$$

where

$$S_1(r, x_{\text{dis}}) = s_1 r^{10} + s_2 r^8 x_{\text{dis}}^2 + s_3 r^6 x_{\text{dis}}^4 + s_4 r^4 x_{\text{dis}}^6 + s_5 r^2 x_{\text{dis}}^8 + s_6 x_{\text{dis}}^{10}$$

$$S_2(r, x_{\text{dis}}) = s_7 r^8 - s_7 r^6 x_{\text{dis}}^2 + s_8 r^4 x_{\text{dis}}^4 + s_9 r^2 x_{\text{dis}}^6 + s_{10} x_{\text{dis}}^8 \quad ,$$

with coefficients given in Table 2:

	i				
	1	2	3	4	5
s_i	1.5	-2.25	1.3125	-0.375	0.0527344
s_{5+i}	-0.00292969	0.125	0.046875	-0.0078125	0.000488281

Table 2. The coefficients of polynomials S_1 and s_2 appearing in (25).

Ultimately, a real solution of (24) which satisfies (25) signifies the existence of a Hopf bifurcation, and becomes the critical value for the bifurcation parameter σ.

5. VALIDATION

5.1 Simulation results

Consider two limit cycles generated by (9) when parameterized with $r = 1.4$ and $x_{\text{dis}} = 2.5$ (Fig. 2).

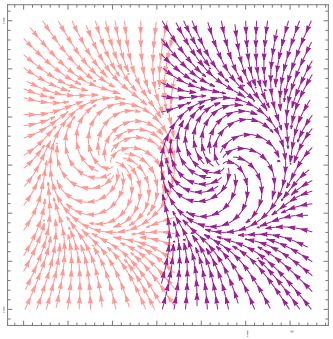

Fig. 2. Component intersecting vector fields F_1 and F_2 as limit cycles of radii $r = 1.4$ and with centers $x_{\text{dis}} = 2.5$ apart.

Proposition 1 predicts a deadlock located at $w_d = (1.25, 0)^\intercal$. At $(x_{\text{dis}}, r) = (2.5, 1.4)$, the critical bifurcation parameter is found to be $\sigma_c = 0.0434$, satisfying both conditions of (Guckenheimer and Holmes, 1983, Theorem 3.4.2) since the the eigenvalues of the Jacobian (17) turn out as:

$$\lambda_{1,2} = \pm 0.788\, i \quad \lambda_3 = -2.337 \quad \frac{\mathrm{d}\lambda}{\mathrm{d}\sigma}\Big|_{\sigma=0.0434} = -7.9 \neq 0 \quad .$$

When $\sigma < \sigma_c$, the trajectories of the navigation dynamics (15) converge to a point attractor. When $\sigma > \sigma_c$, the trajectories of (15) converge to a (new) limit cycle —distinct from F_1 and F_2.

So now select the robot control inputs in (3) to match the vector field of the navigational (slow) dynamics (15), $\nu_x := \dot{w}_1$, $\nu_y := \dot{w}_2$, steering the robot along the composed vector field, which is going to be switching as it goes through bifurcations.

The application scenario is as follows: (i) $t = 0$ seconds: initialize $\Delta m := 1$ to produce a field F_1 with a circular limit cycle centered at the origin; keep Δm fixed for the next 20 seconds. (ii) $t = 20$ seconds: reset $\Delta m := -1$ and keep it constant for another 20 seconds; now the field changes to F_2, a circular limit cycle centered at $(2.5, 0)$. (iii) $t = 40$ seconds: endow Δm with dynamics (15) with $\sigma = 0.05$; the resulting vector field is now a limit cycle around the deadlock $(1.25, 0)$. (iv) $t = 60$ seconds: the bifurcation parameter switches below its critical value to $\sigma = 0.03$, and consequently the vector field becomes a stable node for the deadlock $(1.25, 0)$ The trajectory of a simulated robot tracking the flow lines of the switching field over time is shown in Fig 3. Note how this robot switches dynamical behaviors three times, and yet no instability nor nonsmooth behavior occurs during the transitions.

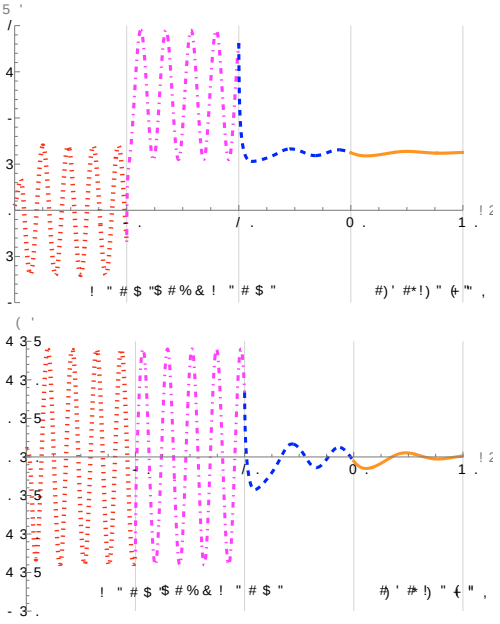

Fig. 3. Simulation results: Evolution of navigation dynamics over time. From $t_0 = 0$ s to $t_1 = 20$ s the robot is following the circular field centered at the origin. At $t_1 = 20$ s its behavior changes and the robot is moving on the second circular field centered at $(2.5, 0)$ until $t_2 = 40$ s when it switches to following a limit cycle around the deadlock $(1.25, 0)$. Lastly, at $t_3 = 60$ s and until $t_4 = 80$ s, the robot is converging to the deadlock.

5.2 Experimental results

The robot used for the experimental study is is a Sphero Bolt (Fig. 1). Its LED array is used to localize it via a Zed overhead camera through color detection. The robot is steered along the vector field of the navigational dynamics, and control commands in the form of speed and direction are sent over bluetooth. The experimental setup mirrors the simulation scenario: the robot is first steered along circular limit cycle centered at the origin fixing $\Delta m := 1$. Then at time $t = 20$ s the reference vector field switches to a circular limit cycle centered at $(x_{\text{dis}}, 0)$, where it rotates for another 20 seconds while $\Delta m := -1$. At time $t = 40$ s Δm is left to evolve according to the motivational dynamics, with $\sigma = 0.05$, which leads the robot to follow an elliptical limit cycle trajectory around the deadlock $(x_{\text{dis}}/2, 0)$. The robot stays on this limit cycle for another 20 seconds after which the bifurcation parameter is reset below the critical value to $\sigma = 0.03$, and the robot now leaves this elliptical track to converge to the deadlock (Fig. 4). Due to the accuracy limitations of the color detection method, and the textured surface on which these robots move (Fig. 1a), the recorded measurements shown in Fig 4 are noisy. Nevertheless, the periodicity of the steady state behaviors is visible and the range of oscillations match the shape and size of the different limit cycles.

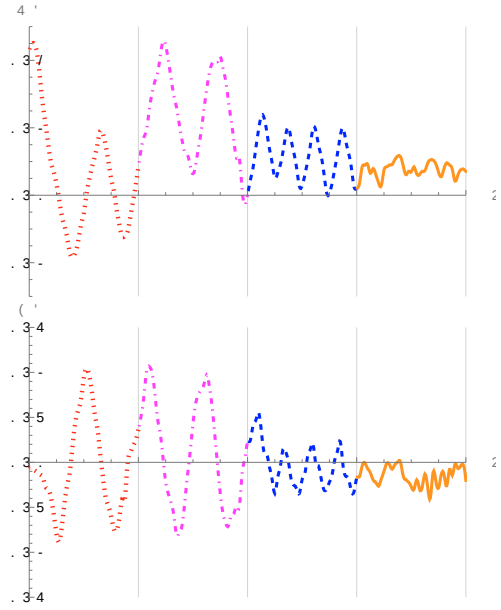

Fig. 4. Experimental results: Evolution of navigation dynamics over time. From $t_0 = 0$ to $t_1 = 20s$ the agent is following the circular field centered at the origin. At $t_1 = 20s$ the behavior changes and the agent is moving on the second circular field centered at $(2.5, 0)$ until $t_2 = 40s$ when it switches to a limit cycle around the deadlock $(1.25, 0)$. Lastly, at $t_3 = 60s$ and until $t_4 = 80s$, the agent is following a convergent behavior at the deadlock.

6. CONCLUSIONS AND FUTURE WORK

This paper realizes the potential of tunable navigational dynamics to steer robots while switching their dynamical behavior using certain types of bifurcations. The dynamical system analysis of the system as it undergoes the bifurcation is performed in the context of singular perturbation theory. The analysis yields closed-form analytical expressions for the critical value of bifurcation parameter, informing the designer on how exactly to reset a single value in the equations of motion in order to trigger the switch in the dynamical behavior. The theoretical predictions are verified through simulation results, and experimental implementation demonstrates the ability of a robot to switch smoothly between a range of different dynamical behaviors.

REFERENCES

Baxevani, K. and Tanner, H.G. (2023). Multi-behavioral multi-robot systems driven by motivation dynamics. *In Proceedings of the IEEE American Control Conference (in print)*.

Baxevani, K. and Tanner, H.G. (2021). Constructing continuous multi-behavioral planar systems through motivation dynamics and bifurcations. In *Proceedings of the IEEE Conference on Decision and Control*, 1095–1100.

Branicky, M. (1998). Multiple Lyapunov functions and other analysis tools for switched and hybrid systems. *IEEE Transactions on Automatic Control*, 43(4), 475–482.

Fainekos, G., Kress-Gazit, H., and Pappas, G. (2005). Temporal logic motion planning for mobile robots. In *Proceedings of the IEEE Conference on Robotics and Automation*, 2020–2025.

Goebel, R., Sanfelice, R.G., and Teel, A.R. (2012). *Hybrid Dynamical Systems*. Princeton University Press.

Guckenheimer, J. and Holmes, P. (1983). *Nonlinear Oscillations, Dynamical Systems, and Bifurcation of Vector Fields*. Springer-Verlag.

Kokkoni, E., Mavroudi, E., Zehfroosh, A., Galloway, J.C., Vidal, R., Heinz, J., and Tanner, H.G. (2020). GEARing smart environments for pediatric motor rehabilitation. *Journal of NeuroEngineering and Rehabilitation*, 17(16), 1–15.

Kokkoni, E., Zehfroosh, A., Kannappan, P., Mavroudi, E., Galloway, J.C., Heinz, J., Vidal, R., and Tanner, H.G. (2017). Principles for building "smart" learning environments in pediatric early rehabilitation. *Robotics: Science and Systems; Workshop on Perception and Interaction Dynamics in Child-Robot Interaction*.

Kouvoutsakis, G., Baxevani, K., Tanner, H.G., and Kokkoni, E. (2022). Feasibility of using the robot sphero to promote perceptual- motor exploration in infants. In *Proceedings of the ACM/IEEE International Conference on Human-Robot Interaction*, 850–854.

Kress-Gazit, H., Fainekos, G.E., and Pappas, G.J. (2007). Where's waldo? sensor-based temporal logic motion planning. In *Proceedings of the IEEE International Conference on Robotics and Automation*, 3116–3121.

Liberzon, D. (2003). *Switching in Systems and Control*. Birkhauser.

Lygeros, J., Johansson, K., Simić, S., and Sastry, S. (2003). Dynamical properties of hybrid automata. *IEEE Transactions on Automatic Control*, 48(1), 2–17.

Pais, D., Hogan, P.M., Schlegel, T., Franks, N.R., Leonard, N.E., and Marshall, J.A. (2013). A mechanism for value-sensitive decision-making. *PloS one*, 8(9), e73216.

Reverdy, P.B. (2019). A route to limit cycles via unfolding the pitchfork with feedback. In *Proceedings of the American Control Conference*, 3057–3062.

Reverdy, P.B. and Koditschek, D.E. (2018). A dynamical system for prioritizing and coordinating motivations. *SIAM Journal of Applied Dynamical Systems*, 17(2), 1683–1715.

Tanner, H.G. and Boddu, A. (2012). Multi-agent navigation functions revisited. *IEEE Transactions on Robotics*, 28(6), 1346–1359.

Thompson, C. and Reverdy, P.B. (2019). Drive-based motivation for coordination of limit cycle behaviors. In *Proceedings of the IEEE Conference on Decision and Control*, 244–249.

Valbuena, L.R. and Tanner, H.G. (2012). Hybrid potential field based control of differential drive mobile robots. *Journal of Intelligent & Robotic Systems*, 68(3), 307–322.

Valbuena, L.R. and Tanner, H.G. (2015). Flocking, formation control and path following for a group of mobile robots. *IEEE Transactions on Control Systems Technology*, 23(4), 1268–1282.

van der Schaft, A.J. and Schumacher, H. (2000). *An Introduction to Hybrid Dynamical Systems*. Springer.

Veer, S., Rakesh, and Poulakakis, I. (2019). Input-to-state stability of periodic orbits of systems with impulse effects via Poincare analysis. *IEEE Transactions on Automatic Control*, 64(11), 4583–4598.

Zehfroosh, A. and Tanner, H.G. (2019). Reactive motion planning for temporal logic tasks without workspace discretization. In *Proceedings of the IEEE American Control Conference*, 4872–4877.

Zehfroosh, A. and Tanner, H.G. (2022). Nonsmooth control barrier navigation functions for STL motion planning. *Frontiers in Robotics and AI*, 9.

Zhong, Y.D. and Leonard, N.E. (2019). A continuous threshold model of cascade dynamics. In *Proceedings of the IEEE Conference on Decision and Control*, 1704–1709.